Biochemical and Biophysical Research Communications 811 (2026) 153535

Contents lists available at ScienceDirect

Biochemical and Biophysical Research Communications

journal homepage: www.elsevier.com/locate/ybbrc

Quantitative analysis of ternary complex kinetics by a surface immobilization method

Xiaohan Mai [a,b], Yang Luo [c], Ruoxin Fang [a], Haina Zhang [a], Lan Mi [a], Jiong Ma [a], Xiangdong Zhu [d], Yu Ding [b,c,*], Yiyan Fei [a,b,**]

[a] Shanghai Engineering Research Center of Ultra-precision Optical Manufacturing, Key Laboratory of Micro and Nano Photonic Structures (Ministry of Education), College of Future Information Technology, Fudan University, Shanghai, 200433, China
[b] Quzhou Fudan Institute, 108 Minjiang Avenue, Kecheng District, Quzhou, Zhejiang Province, China
[c] State Key Laboratory of Genetics and Development of Complex Phenotypes, School of Life Sciences, Fudan University, Shanghai, 200433, China
[d] Department of Physics, University of California, One Shields Avenue, Davis, CA, 95616, USA

ARTICLE INFO

Keywords:
Target protein degradation
Ternary complex kinetics
Hook effect
Cooperativity factor
Oblique-incidence reflectivity difference

ABSTRACT

Targeted protein degradation via bifunctional molecules represents a promising therapeutic strategy, where successful degradation requires efficient ternary complex formation. This study establishes an integrated framework for reliable kinetic characterization of ternary complexes by combining theoretical modeling with experimental validation. We demonstrate that binary binding parameters can effectively guide experimental design, while proper component immobilization and the use of calibrated concentrations of pre-formed binary complexes ensure measurement accuracy. Application to the CRBN/ARV-825/BRD4 system reveals strong positive cooperativity ($\alpha = 175$), which correlates with exceptional degradation potency. Our approach provides a systematic methodology for quantifying ternary complex kinetics and offers a robust platform for rational degrader optimization through kinetic-guided design.

1. Introduction

Target protein degradation (TPD) is an emerging therapeutic strategy that uses small molecules to hijack endogenous cellular degradation pathways for inducing protein degradation. Unlike conventional inhibitors that merely block component activity, TPD directly eliminates target proteins of interest (POIs), offering a promising approach for treating cancer, neurodegenerative diseases, and other pathologies [1–7].

TPD operates through multiple mechanisms, among which bifunctional molecules represent a promising modality. These molecules, such as proteolysis-targeting chimeras (PROTACs), consist of two ligands connected by a linker, with one ligand binds to a POI and another that recruits an E3 ubiquitin ligase, thereby facilitating polyubiquitination and subsequent proteasomal degradation of the POI [4,5]. Similarly, autophagy-tethering compounds (ATTECs) have been developed to bind both the autophagy-related protein LC3 and a pathogenic protein like mutant huntingtin (mHTT), leveraging lysosomal degradation pathways [6].

A hallmark of bifunctional degraders is the characteristic "hook effect" in their concentration-response profiles, where maximal degradation of the target protein is achieved at intermediate concentrations and declines at higher doses. This phenomenon arises because excessive degrader concentrations lead to the saturation of either the target protein or the recruited effector protein, forming non-productive binary complexes and thus preventing the formation of the productive ternary complex necessary for degradation. Notably, the "hook effect" varies in intensity across different degrader systems. These concentration-dependent behaviors directly influence the therapeutic window and dosing regimen, making their understanding critical for developing clinically viable degraders [8,9].

Recent studies have established that the degradation profile of bifunctional degraders is governed by the binary K_d^{binary} and ternary $K_d^{ternary}$ equilibrium dissociation constants, along with their ratio defined as the cooperativity factor $\alpha = K_d^{binary}/K_d^{ternary}$ Here, $\alpha > 1$ denotes

* Corresponding author. Quzhou Fudan Institute, 108 Minjiang Avenue, Kecheng District, Quzhou, Zhejiang Province, China.
** Corresponding author. Shanghai Engineering Research Center of Ultra-precision Optical Manufacturing, Key Laboratory of Micro and Nano Photonic Structures (Ministry of Education), College of Future Information Technology, Fudan University, Shanghai, 200433, China.
E-mail addresses: yuding@fudan.edu.cn (Y. Ding), fyy@fudan.edu.cn (Y. Fei).

https://doi.org/10.1016/j.bbrc.2026.153535
Received 8 December 2025; Received in revised form 6 February 2026; Accepted 26 February 2026
Available online 26 February 2026

positive cooperativity, which stabilizes the ternary complex, while $\alpha < 1$ denotes negative cooperativity, which destabilized it [8–17]. Additionally, the ternary complex dissociation rate constant $k_{off}^{ternary}$ has been shown to influence the initial degradation rate, thereby affecting the time required for degraders to exert their effects [11]. Therefore, a comprehensive characterization of both equilibrium and kinetic parameters is indispensable for the rational degrader design and for elucidating their mechanism of action.

While characterization of binary binding is relatively straightforward, methods for determining ternary $K_d^{ternary}$ and $k_{off}^{ternary}$ remain technically challenging [13]. Several solution-based techniques, such as time-resolved fluorescence energy transfer (TR-FRET), fluorescence polarization (FP) and isothermal titration calorimetry (ITC), have been employed to measure ternary complex equilibrium dissociation constants $K_d^{ternary}$ [9,10,12,17]. In addition, surface-based analytical methods including biolayer interferometry (BLI) and surface plasmon resonance (SPR) enable direct measurement of kinetic rate constants while also providing equilibrium constant information through kinetic analysis with immobilized target proteins [10,11,15,17]. However, accurate characterization of $K_d^{ternary}$ and $k_{off}^{ternary}$ remains challenging due to the intricate concentration dependence inherent to ternary complex formation, where the system exhibits a non-monotonic response to concentration variations across all three components, combined with the complicating effects of the hook phenomenon. Consequently, the reliance on simply using higher concentration often leads to suboptimal conditions, making the systematic identification of optimal concentrations a central methodological difficulty.

To address this challenge, we developed a theoretical and experimental framework based on readily measurable binary equilibrium dissociation constants K_d^{binary} to provide optimal conditions for ternary complex formation. This framework establishes a direct correlation between K_d^{binary} values and optimal concentrations for maximal ternary complex yield, while also defining the specific conditions under which the 1:1 Langmuir model remains applicable to ternary interactions. Our results identify three essential elements for accurate kinetic characterization: implementation of pre-incubation protocols, strategic selection of the immobilized protein component, and verification that the system satisfies the fundamental cooperativity condition. Experimental validation using the Cereblon (CRBN)/ARV-825/BRD4 model system with an oblique-incidence reflectivity difference (OI-RD) biosensor confirmed these theoretically derived principles.

2. Materials and methods

2.1. Kinetic and equilibrium parameters in bifunctional degrader-induced ternary systems

Fig. 1 illustrates a ternary interaction system induced by a bifunctional degrader (molecule B). The system comprises binary interactions between molecule A and B, and between molecule B and C. The association rate constant for forming the binary complex AB is denoted as $k_{on,AB}^{binary}$, while its dissociation rate constant is represented by $k_{off,AB}^{binary}$. The corresponding equilibrium dissociation constant between molecule A and B is defined as $K_{d,AB}^{binary}$. These kinetic and equilibrium parameters follow the same nomenclature for the BC interaction, with $k_{on,BC}^{binary}$, $k_{off,BC}^{binary}$, and $K_{d,BC}^{binary}$ describing the formation, dissociation, and equilibrium properties of the BC complex, respectively.

The system also features interactions involving the pre-formed binary complex. These include the association between binary complex BC and molecule A, as well as between binary complex AB and molecule C. The formation of ternary complex ABC from binary complex BC and molecule A is characterized by the associate rate constant $k_{on,A-BC}^{ternary}$ and the corresponding dissociation rate constant $k_{off,A-BC}^{ternary}$. The equilibrium dissociation constant for this ternary interaction is denoted as $K_{d,A-BC}^{ternary}$. Similarly, the parameters $k_{on,AB-C}^{ternary}$, $k_{off,AB-C}^{ternary}$, and $K_{d,AB-C}^{ternary}$ describe the ternary interaction between complex AB and molecule C. With the binary and ternary dissociation constants, the cooperativity factor can be calculated as a fundamental relationship expressed as $\alpha =$

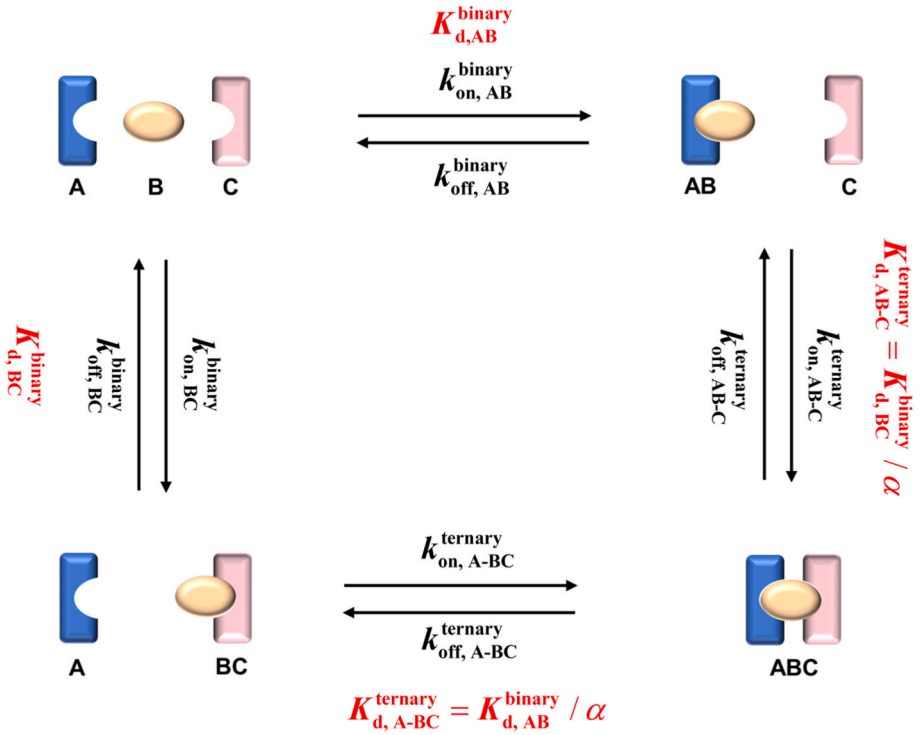

Fig. 1. Schematic of the ternary interaction system and its associated kinetic and equilibrium parameters.

$K_{d,AB}^{binary}/K_{d,A-BC}^{ternary}$ and $\alpha = K_{d,BC}^{binary}/K_{d,AB-C}^{ternary}$, respectively [8,9].

2.2. Reagents and materials

Cereblon (CRBN) was purchased from Abmart (Shanghai, China). ARV-825 was purchased from Selleck (Shanghai, China). Bovine Serum Albumin (BSA) was purchased from Sigma-Aldrich Co. (Shanghai, China). Isocyanate-functionalized slides were prepared following the established protocol described by Zhu et al. [18] Epoxy functionalized slides were purchased from Capital Bio Technology Co., Ltd (Beijing, China). Dimethyl Sulfoxide (DMSO) was purchased from Sinopharm Chemical Reagent Company (Shanghai, China).

The human BRD4 (BRD4 bromodomain 1, residues 44–168 based on UniProt O60885) was cloned into a pRSFDuet-1–based vector containing an N-terminal His_{10}-SUMO tag and expressed in *E. coli* BL21 (DE3). Cells were cultured in LB medium and induced at 18 °C overnight with 0.2 mM IPTG. Cells were harvested by centrifugation and resuspended in NiA buffer (50 mM Tris-HCl, 150 mM NaCl, 20 mM imidazole, 5% glycerol, pH 7.5), lysed by sonication, and clarified by centrifugation. The BRD4 protein was purified via Ni-NTA, followed by His_{10}-SUMO tag cleavage using ULP1 protease, then concentrated and subjected to size-exclusion chromatography on a Superdex 200 Increase column in gel-filtration buffer (20 mM HEPES, 150 mM NaCl, pH 7.5).

2.3. Microarray fabrication

A small molecule microarray was prepared by dispensing ARV-825 (10 mM in DMSO) onto isocyanate-functionalized slides using a SmartArrayer 136 microarray spotter (CapitalBio Corporation, Beijing). Each array comprised 12 spots with diameters of 100-150 μm and center-to-center spacing of 300 μm. After printing, these slides were dried at 45 °C for 24 h and stored at −20 °C until further use.

For protein microarray preparation, CRBN was diluted to 0.5 mg/mL in HEPES buffer (pH 7.5) and printed onto epoxy-functionalized slides using a Super Marathon printer (Arrayjet, UK) under controlled conditions (20 °C, 50% relative humidity). Each array consisted of 8 spots, with each spot formed by depositing two 100 pL per droplets. The resulting spots measured approximately 130 μm in diameter, with a center-to-center spacing of 300 μm. The printed slides were stored at 4 °C until use.

2.4. Binary and ternary kinetics characterization with OI-RD biosensor

The binding kinetics of binary and ternary complexes formed by CRBN, ARV-825, and BRD4 were characterized using the OI-RD biosensor [19–24], a label-free detection technology that monitors biomolecular interactions in real time via changes in optical film thickness. All assays were performed in a surface-based configuration with one interaction partner immobilized on the slide.

Prior to detection, the biochip was placed in a fluid chamber and equilibrated with HEPES buffer until no molecular desorption was observed. Residual reactive sites on the chip were subsequently blocked by treating the surface with 7.5 μM BSA in HEPES for 30 min. Real time binding measurements began with a 10 min HEPES buffer flow at 0.004 mL/min to establish a stable baseline. Sample injection was performed in two stages, beginning with a rapid introduction at 1.176 mL/min for 20 s, followed by a 30 min association phase at 0.004 mL/min. Dissociation was initiated by switching back to HEPES buffer at 1.18 mL/min for 20 s, after which the dissociation process was monitored for 30 min under continuous HEPES buffer flow at 0.004 mL/min. All measurements included image acquisition before and after the detection cycle.

For ternary binding assays, BRD4 and ARV-825 were pre-incubated for 1–1.5 h to ensure formation of the binary complex prior to injection over the immobilized CRBN surface. All other experimental conditions, including flow rates, buffer composition, and detection parameters, remained consistent with the binary binding assays.

3. Results

3.1. Equilibrium analysis of ternary complex formation

We first investigated how the equilibrium concentration of the ternary complex is influenced by the concentrations of component B and C, as well as the cooperativity factor α, in a surface-based assay configuration with immobilized component A. This configuration results in a very low effective concentration of component A due to the limited binding sites available on the substrate.

Fig. 2(a) shows the normalized $[ABC]/[A]_t$ as a function of $[B]_t$ and $[C]_t$, obtained by numerically solving the equilibrium equations (Text S1). Here, $[A]_t$, $[B]_t$, and $[C]_t$ represent total concentrations, while [ABC] denotes the equilibrium concentration of ternary complex. Simulations were performed using $[A]_t = 1$ nM, $K_{d,AB}^{binary} = 1000$ nM, $K_{d,BC}^{binary} = 100$ nM, and $\alpha = 1$. The results exhibit characteristic hook behavior where at fixed $[C]_t$, the ratio $[ABC]/[A]_t$ initially increases and then deceases with increasing $[B]_t$. Moreover, increasing $[C]_t$ raises both the maximum ternary complex concentration ($[ABC]_{max}$) and the required $[B]_t$ required to achieve it ($[B]_{t,\ ABC\text{-}max}$), as marked by the red stars, indicating that higher C concentration enhance ternary complex formation but also demand more B for optimal yield.

Based on simulations performed at a fixed $[C]_t$ of 1000 nM, we further investigated the effect of α on ternary complex formation. As shown in Fig. 2(b), increasing α not only enhances the yield of the ternary complex but also broadens the range of $[B]_t$ that supports substantial complex formation. When α is sufficiently high, the ratio $[ABC]/[A]_t$ approaches unity, indicating nearly complete recruitment of component A into the ternary complex. Notably, $[B]_{t,\ ABC\text{-}max}$ remains invariant with α, as illustrated by the vertical dashed line in Fig. 2(b). This key finding demonstrates that the concentration of B required for maximum ternary complex formation can be predicted using only the K_d^{binary} values, independent of α or the $K_d^{ternary}$.

Maximizing ternary complex formation serves as an effective strategy to enhance signal, thereby facilitating the measurement of ternary binding interactions. When this strategy is employed, it necessitates the precise determination of both $[ABC]_{max}$ and the corresponding $[B]_{t,\ ABC\text{-}max}$. By analyzing the equilibrium equations under the extremum condition $d[ABC]/d[B]_t = 0$, we derived analytical solutions for these two key parameters (Text S1), as given in Eq. (1)and Eq. (2).

$$\frac{[ABC]_{max}}{[A]_t} \approx \frac{\alpha[C]_t}{\alpha[C]_t + \left(\sqrt{K_{d,AB}^{binary}} + \sqrt{K_{d,BC}^{ternary}}\right)^2} \tag{1}$$

$$\frac{[B]_{t,ABC-max}}{[C]_t} \approx \frac{\sqrt{K_{d,AB}^{binary} K_{d,BC}^{binary}}}{[C]_t} + \frac{\sqrt{K_{d,AB}^{binary}}}{\sqrt{K_{d,AB}^{binary}} + \sqrt{K_{d,BC}^{binary}}} \tag{2}$$

Eq. (1) provides an analytical expression for $[ABC]_{max}/[A]_t$, showing that the ternary complex yield is governed by the product of $\alpha[C]_t$. This relationship is corroborated by SPR data [15] and Fig. 2(c), where larger values of this product correspond to higher ternary complex yields. Since α is an intrinsic system property, increasing $[C]_t$ is the primary experimental lever for enhancing yield. This strategy is system-dependent that highly cooperative systems with large α achieve significant yield at modest $[C]_t$, whereas weakly cooperative ones require higher $[C]_t$. Consequently, when the cooperativity factorα is unknow, systematically increasing $[C]_t$, provides the most reliable and generally applicable strategy for signal enhancement.

Eq. (2) provides an analytical expression for the ratio $[B]_{t,\ ABC\text{-}max}/[C]_t$, demonstrating its dependence on the binary equilibrium

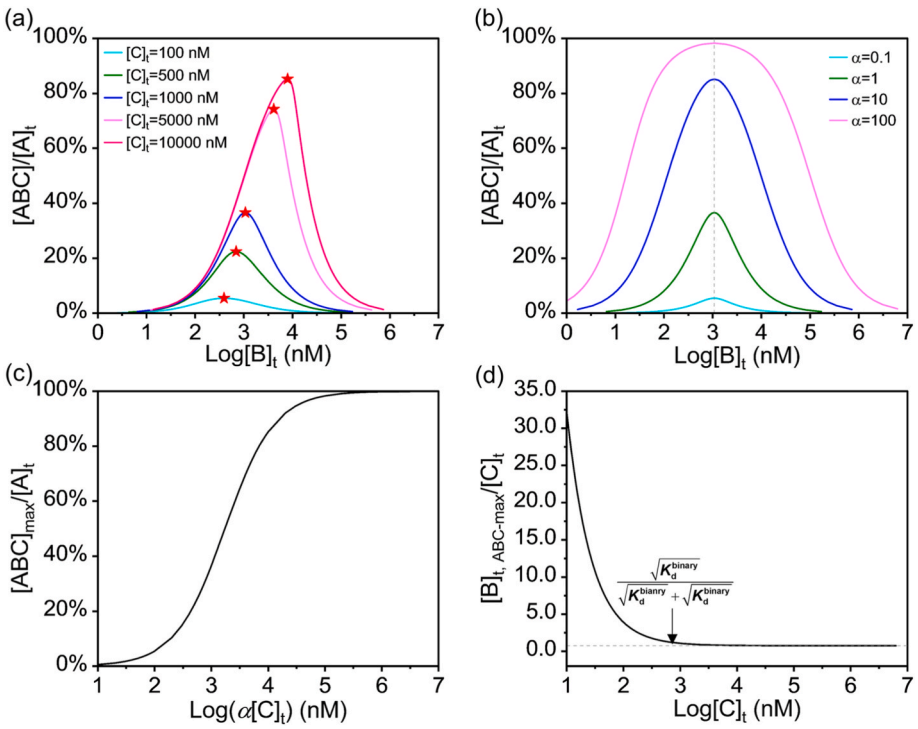

Fig. 2. Numerical fitting based on equilibrium equations. (a) Dependence of normalized ternary complex formation on degrader concentration at different $[C]_t$ level. Red stars indicate $[ABC]_{max}$. (b) Influence of α on normalized ternary complex formation. The dashed line highlights the constant $[B]_t$ required for $[ABC]_{max}$ across all α values. (c) Correlation between the maximum ternary complex yield and the product $\alpha[C]_t$. (d) Evolution of the ratio $[B]_{t,\ ABC\text{-}max}/[C]_t$ ratio with increasing $[C]_t$. (For interpretation of the references to colour in this figure legend, the reader is referred to the Web version of this article.)

dissociation constants $K_{d,AB}^{binary}$ and $K_{d,BC}^{binary}$, as well as the concentration $[C]_t$, but not on α. This result aligns with the form derived by Douglass et al. [8] under the specified approximations under low $[A]_t$ approximations. Fig. 2(d) illustrates how the ratio varies with $[C]_t$, revealing a characteristic transition across concentration regimes. When $[C]_t$ is much smaller than $\sqrt{K_{d,AB}^{binary}K_{d,BC}^{binary}}$, the ratio is much greater than 1, indicating that B must be in significant excess. As $[C]_t$ increases, this ratio decreases monotonically. When $[C]_t$ substantially exceeds $\sqrt{K_{d,AB}^{binary}K_{d,BC}^{binary}}$, the ratio plateaus at a constant value of $\sqrt{K_{d,AB}^{binary}}/\left(\sqrt{K_{d,AB}^{binary}}+\sqrt{K_{d,BC}^{binary}}\right)$. This limiting value is always less than 1, indicating that the optimal concentration B is lower than that of C under high-concentration conditions.

3.2. Optimizing kinetic measurement of ternary complex binding

To quantitatively determine the cooperativity factor α, we employed the experimental configuration shown in Fig. 1, where protein A is immobilized on the sensor surface and the pre-formed BC complex is introduced as the flowing analyte. Applying the 1:1 Langmuir binding model to this ternary system requires treating BC complex as a single analyte, which necessitates maintaining a nearly constant concentration of BC complex throughout the measurement to obtain reliable kinetic parameters [25].

We systematically evaluated this requirement by simulating the ternary system using kinetic equations (Text S2). As shown in Fig. 3(a), simulations performed at B and C concentrations that maximize the ternary complex formation confirm that pre-incubation of B and C before injection (black curve) maintains a constant [BC] level, whereas simultaneous introduction of B and C (blue curve) leads to progressive accumulation of [BC]. These results establish that pre-incubation is

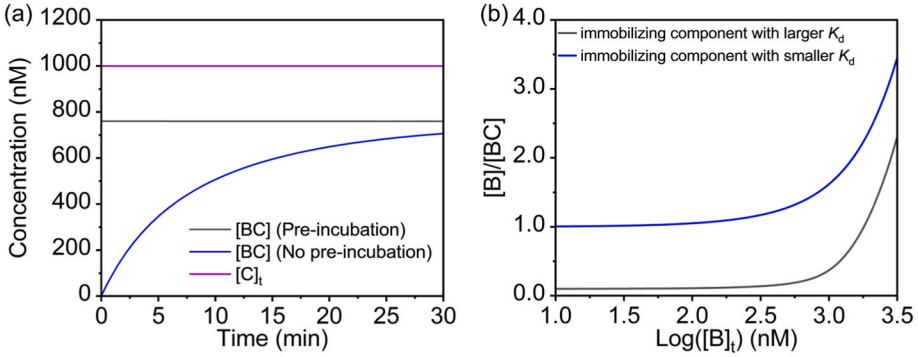

Fig. 3. (a) Temporal profile of [BC] in the flow phase over immobilized A under pre-incubation and simultaneous injection conditions. (b) Dependence of the [B]/[BC] ratio on the choice of immobilized component.

essential to meet the constant analyte concentration requirement for valid 1:1 kinetic analysis.

Furthermore, Fig. 3(a) also shows that under optimal conditions with comparable concentrations of B and C, the equilibrium [BC] is substantially lower than $[C]_t$. This finding invalidates the common practice of substituting the limiting component's concentration for [BC], an approximation only valid when one component is in large excess. Accurate determination of the ternary equilibrium dissociation constant $K_{d,A-BC}^{ternary}$ therefore requires using the actual [BC] values. This calibration reconciles data from experiments with similar component concentrations with those using component excess, resolving inconsistencies in Roy et al. [11]

A second prerequisite for valid 1:1 Langmuir analysis is that the reaction follows a single dominant pathway, where immobilized A bind predominantly to the pre-formed BC complex rather than to free B. This condition is reasonably satisfied when the equilibrium [AB] is negligible compared to the ternary complex ([AB] ≪ [ABC]), which can be simplified to the inequality in Eq. (3) (Text S3):

$$\frac{[B]}{[BC]} \ll \alpha \tag{3}$$

here, [BC] denotes the equilibrium concentration of the BC complex in the pre-incubated mixture, calculated as (Text S3):

$$[BC] = \frac{[B]_t + [C]_t + K_{d,BC}^{binary} - \sqrt{\left([B]_t + [C]_t + K_{d,BC}^{binary}\right)^2 - 4[B]_t[C]_t}}{2} \tag{4}$$

and [B] is the corresponding equilibrium concentration of unbound B.

Fig. 3(b) shows how the ratio [B]/[BC], derived from Eq. (4), varies with the concentration of B and the choice of immobilized component. The larger and smaller K_d^{binary} equal to 1000 nM and 100 nM, respectively. The results show that immobilizing the weaker-binding component (with larger $K_{d,AB}^{binary}$) yields a lower [AB]/[ABC] ratio, reducing the demand for high cooperativity factor α by facilitating satisfaction of Eq. (3). In previous PROTAC ternary studies, the choice of immobilization target has often been arbitrary, driven by practical convenience [13]. Notably, Roy et al. [11] found that successful kinetic fitting was only achievable when the weaker-binding component was immobilized. Our work now provides the kinetic rationale for this observation that the weaker-binding component should be immobilized to ensure clean 1:1 Langmuir kinetics.

Fig. 3(b) further shows that reducing the concentration of component B lowers the [B]/[BC] ratios, thereby reducing the minimum α required to satisfy Eq. (3). This explains the widespread use of C in excess, though such conditions often yield weaker signals. At optimal concentration for maximum ternary formation, the required α threshold is substantially higher. Therefore, after experimentally determining α, it is essential to verify that the system satisfies the cooperativity condition by comparing the measured α value with the theoretically threshold derived from [B]/[BC]. A measured α that exceeds the threshold validates the simplified model, whereas failure indicates substantial direct binding between the immobilized A and free B, compromising result reliability.

Under the optimized experimental conditions established above, kinetic fitting using 1:1 Langmuir model was applied to determine the apparent ternary equilibrium dissociation constant $K_{d,A-BC}^{ternary}$. The cooperativity factor was then calculated as $\alpha = K_{d,AB}^{binary}/K_{d,A-BC}^{ternary}$, where $K_{d,AB}^{binary}$ was obtained from independent binary binding measurements.

3.3. Kinetic characterization of ternary complex in biologically relevant system

Guided by our theoretical framework for ternary complex formation, we performed kinetic characterization of the CRBN/ARV-825/BRD4 model system using an OI-RD biosensor. The bifunctional degrader ARV-825 contains pomalidomide (targeting CRBN) linked to OTX015 (target BRD4) through a flexible spacer, enabling simultaneous engagement of E3 ubiquitin ligase CRBN and target protein BRD4 [26]. In accordance with the theoretical predictions, we employed optimized component concentrations and immobilization strategies for real-time kinetic measurements of the ternary interaction.

We first characterized the binary kinetics between ARV-825 and its binding partners. With ARV-825 immobilized on the sensor surface, we measured its interaction with concentration gradients of CRBN (240, 500, and 600 nM) and BRD4 (200, 1500 and 2000 nM), with upper concentration limits determined by nonspecific binding observed in preliminary tests. The binding curves, as shown in Fig. 4(a) and (b), yield $K_d^{binary} = 118 \pm 10$ nM for the BRD4/ARV-825 and $K_d^{binary} = 2810 \pm 295$ nM for the CRBN/ARV-825 (Table S1), consistent with literature values [26].

Following our theoretical finding that immobilizing the weaker-binding component suppresses competing binary interaction, we immobilized CRBN for ternary complex characterization. Binding experiments were conducted at BRD4 concentrations of 100, 200, and 600 nM, paired with optimal ARV-825 concentrations of 660, 740, and 1080 nM, respectively. ARV-825 and BRD4 were pre-incubated for 1.5 h before injection to maintain constant binary complex concentration, as required for valid 1:1 Langmuir analysis.

The binding responses for ternary complex formation are presented in Fig. 4(c). Fitting these curves with the 1:1 Langmuir model using the calibrated concentration of the pre-formed ARV-825/BRD4 complex yielded a ternary equilibrium dissociation constant ($K_d^{ternary}$) of 16.1 ± 2.3 nM, corresponding to a cooperativity factor α of 175. This value substantially exceeds the maximum theoretical α threshold of 69 calculated from [B]/[BC] ratio across all tested concentration, confirming the validity of the kinetic measurement.

This large α value reflects strong positive cooperativity, indicating highly favored formation of the CRBN/ARV-825/BRD4 ternary complex. The pronounced cooperativity provides a plausible explanation for the exceptionally high degradation potency observed in cellular assays ($DC_{50} < 1$ nM). The substantial enhancement in ternary complex stability compared to binary interactions likely facilitates the ubiquitination process, consistent with the potent and rapid target degradation reported in the literature [26].

4. Discussion

This study establishes an integrated theoretical and experimental framework for characterizing ternary complex kinetics in targeted protein degradation systems. Our analysis demonstrates that optimal ternary complex formation can be predicted using binary dissociation constants, while pre-incubation is essential for maintaining constant complex concentrations required for reliable kinetic measurements.

Experimental validation in the CRBN/ARV-825/BRD4 model system revealed strong positive cooperativity ($\alpha = 175$). By immobilizing the weaker-binding component CRBN and verifying satisfaction of condition [B]/[BC]≪ α, we minimized binary pathway interference. Combined with calibrated [BC] under optimal conditions, this approach provides accurate kinetic measurements for ternary formation.

The framework developed here is applicable to ternary complexes across a wide range of cooperativity. Its optimization strategies, including the concentration guidelines, the calibrated use of pre-formed binary complexes, and the immobilization of the weaker-binding component, rest on kinetic principles that are independent of the magnitude of α. Experimental application to the high-α CRBN/ARV-825/BRD4 system verified the accuracy of the approach for quantifying stable ternary complexes. Consequently, the same principles can be directly applied to PROTACs exhibiting negative or neutral

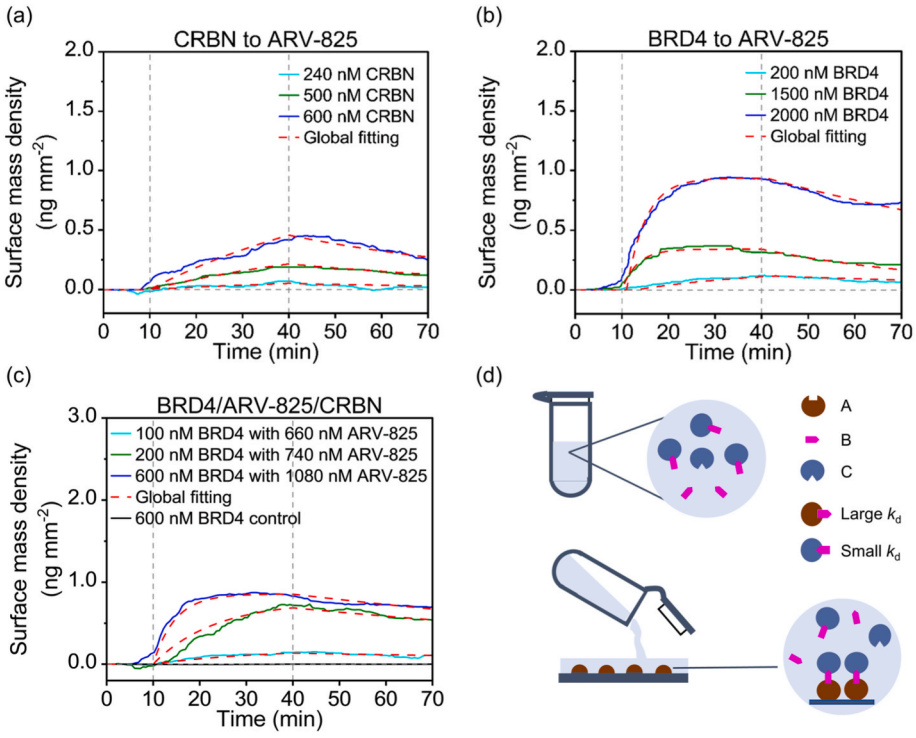

Fig. 4. (a) Binary binding kinetics between immobilized ARV-825 and CRBN at indicated concentrations. (b) Binary binding kinetics between immobilized ARV-825 and BRD4 at indicated concentrations. (c) Ternary binding kinetics between immobilized CRBN and pre-formed ARV-825/BRD4 complex at indicated concentrations. (d) Schematic illustration of the ternary complex detection strategy.

cooperativity, where the underlying dependences of complex yield and kinetics on component concentrations remain unchanged.

A fundamental consideration in our approach concerns the interpretation of kinetic parameters. The measured dissociation rate represents a composite of both possible dissociation pathways (BRD4 release and CRBN release), meaning the calculated cooperativity factor ($\alpha = 175$) should be considered a conservative estimate. This limitation is universal to current ternary complex kinetic analysis techniques, as no existing method can unambiguously distinguish individual dissociation pathways without introducing significant perturbations. Despite this constraint, our methodology provides a robust platform for comparative analysis of ternary complex stability across different degrader systems.

This work provides a methodological foundation for rational degrader design by quantifying how structural factors affect ternary kinetics. The measured α value directly predicts degradation efficacy by reflecting ternary complex stability, offering a practical mechanism-based criterion for candidate prioritization. Although future methods may elucidate individual dissociation pathways, our approach enables effective degrader optimization through kinetic characterization.

5. Conclusion

This study establishes an integrated theoretical and experimental framework for analyzing ternary complex kinetics in targeted protein degradation. We demonstrate that binary binding parameters alone can guide the optimization of ternary complex formation. Through appropriate experimental design including the use of calibrated concentrations of pre-formed binary complexes and strategic immobilization of the weaker-binding component, measurement validity is ensured. Validation in the CRBN/ARV-825/BRD4 system revealed strong positive cooperativity ($\alpha = 175$) that significantly exceeded the theoretical threshold, providing a mechanistic explanation for the observed high degradation potency. Although the measured dissociation rate represents a combined output of multiple pathways, our approach establishes a reliable basis for comparing degrader efficiency and supports rational degrader optimization using kinetic insights.

Declaration of generative AI use

During the preparation of this work the authors used Deepseek for language polishing. After using this tool, the authors reviewed and edited the content as needed and take full responsibility for the content of the published article.

Funding source

This work was supported by National Key Research and Development Program of China (2021YFA0805200), National Natural Science Foundation of China (32271510, 82030106, 62175036, 62175034), National Key Research and Development Program of China (2021YFF0502900) and Shanghai Key Laboratory of Metasurfaces for Light Manipulation (23dz2260100).

CRediT authorship contribution statement

Xiaohan Mai: Data curation, Formal analysis, Investigation, Methodology, Validation, Writing – original draft. **Yang Luo:** Data curation, Formal analysis, Resources, Writing – original draft. **Ruoxin Fang:** Data curation, Formal analysis, Investigation. **Haina Zhang:** Data curation. **Lan Mi:** Resources. **Jiong Ma:** Resources. **Xiangdong Zhu:** Resources, Software. **Yu Ding:** Data curation, Formal analysis, Funding acquisition, Resources, Writing – review & editing. **Yiyan Fei:** Conceptualization, Data curation, Funding acquisition, Project administration, Resources, Software, Supervision, Writing – review & editing.

Declaration of competing interest

The authors declare no competing financial interest.

Abbreviations

TPD, target protein degradation; POIs, proteins of interest; PROTACs, proteolysis-targeting chimeras; ATTECs, autophagy-tethering compounds; mHTT, mutant huntingtin; TR-FRET, time-resolved fluorescence energy transfer; FP, fluorescence polarization; ITC, isothermal titration calorimetry; BLI, biolayer interferometry; SPR, surface plasmon resonance; CRBN, Cereblon; BRD4, Bromodomain protein 4; BSA, bovine serum albumin; OI-RD, oblique-incidence reflectivity difference.

Appendix A. Supplementary data

Supplementary data to this article can be found online at https://doi.org/10.1016/j.bbrc.2026.153535.

References

[1] Y. Ding, D. Xing, Y.Y. Fei, B.X. Lu, Emerging degradation technologies engaging lysosomal pathways, Chem. Soc. Rev. 51 (2022) 8832–8876, https://doi.org/10.1039/D2CS00624C.

[2] G.Q. Dong, Y. Ding, S.P. He, C.Q. Sheng, Molecular glues for targeted protein degradation: from serendipity to rational discovery, J. Med. Chem. 64 (2021) 10606–10620, https://doi.org/10.1021/acs.jmedchem.1c00895.

[3] J. Salami, C.M. Crews, Waste disposal—an attractive strategy for cancer therapy, Science 355 (2017) 1163–1167, https://doi.org/10.1126/science.aam7340.

[4] K.M. Sakamoto, K.B. Kim, A. Kumagai, F. Mercurio, C.M. Crews, R.J. Deshaies, Protacs: chimeric molecules that target proteins to the Skp1-Cullin-F box complex for ubiquitination and degradation, Proc. Natl. Acad. Sci. 98 (2001) 8554–8559, https://doi.org/10.1073/pnas.141230798.

[5] E. Bulatov, A. Ciulli, Targeting Cullin-RING E3 ubiquitin ligases for drug discovery: structure, assembly and small-molecule modulation, Biochem. J. 467 (2015) 365–386, https://doi.org/10.1042/BJ20141450.

[6] Z.Y. Li, C. Wang, Z.Y. Wang, C.G. Zhu, J. Li, T. Sha, L.X. Ma, et al., Allele-selective lowering of mutant HTT protein by HTT–LC3 linker compounds, Nature 575 (2019) 203–209, https://doi.org/10.1038/s41586-019-1722-1.

[7] X.Y. Li, W.C. Pu, Q.C. Zheng, M. Ai, S. Chen, Y. Peng, Proteolysis-targeting chimeras (PROTACs) in cancer therapy, Mol. Cancer 21 (2022) 99, https://doi.org/10.1186/s12943-021-01434-3.

[8] E.F. Douglass Jr., C.J. Miller, G. Sparer, H. Shapiro, D.A. Spiegel, D, A comprehensive mathematical model for three-body binding equilibria, J. Am. Chem. Soc. 135 (2013) 6092–6099, https://doi.org/10.1021/ja311795d.

[9] W.W. Lin, T.S. Chen, General stepwise approach to optimize a TR-FRET assay for characterizing the BRD/PROTAC/CRBN ternary complex, ACS Pharmacol. Transl. Sci. 4 (4) (2021) 941–952, https://doi.org/10.1021/acsptsci.1c00032.

[10] X. Liu, X. Zhang, D. Lv, Y. Yuan, G. Zheng, D. Zhou, Assays and technologies for developing proteolysis targeting chimera degraders, Future Med. Chem. 12 (2020) 1155–1179, https://doi.org/10.4155/fmc-2020-0073.

[11] M.J. Roy, S. Winkler, S.J. Hughes, C. Whitworth, M. Galant, W. Farnaby, et al., SPR-measured dissociation kinetics of PROTAC ternary complexes influence target degradation rate, ACS Chem. Biol. 14 (2019) 361–368, https://doi.org/10.1101/451948.

[12] K.H. Chan, M. Zengerle, A. Testa, A. Ciulli, Impact of target warhead and linkage vector on inducing protein degradation: comparison of bromodomain and extra-terminal (BET) degraders derived from triazolodiazepine (JQ1) and tetrahydroquinoline (I-BET726) BET inhibitor scaffolds, J. Med. Chem. 60 (2017) 10513–10526, https://doi.org/10.1021/acs.jmedchem.6b01912.

[13] J.A. Ward, C. Perez-Lopez, C. Mayor-Ruiz, Biophysical and computational approaches to study ternary complexes: a 'Cooperative Relationship' to rationalize targeted protein degradation, Chembiochem 24 (2023) e202300163, https://doi.org/10.1002/cbic.202300163.

[14] S.J. Hughes, A. Ciulli, Molecular recognition of ternary complexes: a new dimension in the structure-guided design of chemical degradation, Essays Biochem. 61 (2017) 505–516, https://doi.org/10.1042/EBC20170041.

[15] R.P. Wurz, H. Rui, K. Dellamaggiore, S. Ghimire-Rijal, K. Choi, K. Smither, et al., Affinity and cooperativity modulate ternary complex formation to drive targeted protein degradation, Nat. Commun. 14 (2023) 4177, https://doi.org/10.1038/s41467-023-39904-5.

[16] M.S. Gadd, A. Testa, X. Lucas, C.W. Chung, A. Ciulli, Structural basis of PROTAC cooperative recognition for selective protein degradation, Nat. Chem. Biol. 13 (2017) 514–521, https://doi.org/10.1038/nchembio.2329.

[17] W. Jiang, H. Soutter, The development and application of biophysical assays for evaluating ternary complex formation induced by proteolysis targeting chimeras (PROTACS), J. Vis. Exp. 203 (2024) e65718, https://doi.org/10.3791/65718.

[18] C.G. Zhu, X.D. Zhu, J.P. Landry, Z.M. Cui, Q.F. Li, Y.J. Dang, et al., Developing an efficient and general strategy for immobilization of small molecules onto microarrays using isocyanate chemistry, Sensors 16 (2016) 378, https://doi.org/10.3390/s16030378.

[19] Y.Y. Fei, A. Schmidt, G. Bylund, D.X. Johansson, S. Henriksson, C. Lebrilla, et al., Use of real-time, label-free analysis in revealing low-affinity binding to blood group antigens by Helicobacter pylori, Anal. Chem. 83 (2011) 6336–6341, https://doi.org/10.1021/ac201260c.

[20] Y. Y. Fei, J. P. Landry, Y. S. Sun, X. D. Zhu, J. T. Luo, X. B. Wang, et al., A novel high-throughput scanning microscope for label-free detection of protein and small-molecule chemical microarrays. Rev. Sci. Instrum. 79, 013708, https://doi.org/10.1063/1.2830286.

[21] J.P. Landry, Y.Y. Fei, Y.S. Sun, X. D. Simultaneous measurement of 10,000 protein-ligand affinity constants using microarray-based kinetic constant assays, Assay Drug Dev. Technol. 10 (2012) 250–259, https://doi.org/10.1089/adt.2011.0406.

[22] Y. Y, Fei, Y. Sun, Y.H. Li, H. Yu, K. Lau, J.P. Landry, et al., Characterization of receptor binding profiles of influenza A viruses using an ellipsometry-based label-free glycan microarray assay platform, Biomolecules 5 (2015) 1480–1498, https://doi.org/10.3390/biom5031480.

[23] J.P. Landry, Y.S. Sun, X.W. Guo, X.D. Zhu, X.D. Protein, Reactions with surface-bound molecular targets detected by oblique-incidence reflectivity difference microscopes, Appl. Opt. 47 (2008) 3275–3288, https://doi.org/10.1364/AO.47.003275.

[24] M.J. Xu, B.Y. Shi, H.F. Li, X.H. Mai, L. Mi, J. Ma, et al., Development of a carboxymethyl chitosan functionalized slide for small molecule detection using oblique-incidence reflectivity difference technology. Biomed, Opt. Express 15 (2024) 5947–5959, https://doi.org/10.1364/BOE.534563.

[25] I. Jarmoskaite, I. AlSadhan, P.P. Vaidyanathan, D. Herschlag, How to measure and evaluate binding affinities, eLife 9 (2020) e57264, https://doi.org/10.7554/eLife.57264.

[26] J. Lu, Y. Qian, M. Altieri, H.Q. Dong, J. Wang, K. Raina, et al., Hijacking the E3 ubiquitin ligase cereblon to efficiently target BRD4, Chem. Biol. 22 (2015) 120–135, https://doi.org/10.1016/j.chembiol.2015.05.009.